MHD STUDY OF CORONAL WAVES: A NUMERICAL APPROACH

S. PARHI[1], B.P. PANDEY[1], M. GOOSSENS[2], G.S. LAKHINA[1] and P. DE BRUYNE[2]
[1] *Indian Institute of Geomagnetism, Colaba, Bombay 400 005, India*
[2] *Center for Plasma Astrophysics, Katholieke Universiteit Leuven, Celestijnenlaan 200B, B-3001 Leuven, Belgium*

(Received 9 December, 1996; accepted 25 May, 1997)

Abstract. The solar corona, modelled by a low β, resistive plasma slab sustains MHD wave propagations due to footpoint motions in the photosphere. The density, magnetic profile and driver are considered to be neither very smooth nor very steep. The numerical simulation presents the evolution of MHD waves and the formation of current sheet. Steep gradients in slow wave at the slab edges which are signature of resonance layer where dissipation takes place are observed. Singularity is removed by the inclusion of finite resistivity. Dissipation takes place around the resonance layer where the perturbation develops large gradients. The width of the resonance layer is calculated. The thickness of the Alfvén resonance layer is more than that of the slow wave resonance layer. Attempt is made to distinguish between slow and Alfvén wave resonance layers. Fast waves develop into kink modes. As plasma evolves the current sheets which provide the heating at the edges gets distorted and fragment into two current sheets at each edge which in turn come closer when the twist is enhanced.

1. Introduction

It is known that coronal structure is a typical feature of the sun and sun-like stars. The solar corona is a hot, tenuous plasma permeated with the structured magnetic fields. Corona has closed as well as open field topologies. Corona is far from hydrostatic equilibrium and continuously expands in the interplanetary medium as the solar wind. A variety of waves is generated in the corona due to the convective upwelling motions in the photosphere. New magnetic flux emerges from below the photosphere and interacts with the coronal plasma.

The footpoint motion of the field lines in the photosphere can lead to the excitation of MHD fluctuations. Such a study has been conducted in the recent past by several authors (e.g., Steinolfson, 1991; Cadez and Ballester, 1994; Rickard and Priest, 1994). A general disturbance in the photosphere may produce different kinds of waves, e.g., Alfvén waves, fast and slow magnetoacoustic waves as well as current sheets. For sufficiently slow photospheric motion ($\tau > \tau_A = L/V_A$, where V_A is the Alfvén velocity and L is the size of the system) current sheets may play an important role in the coronal heating. A current sheet is formed by photospheric disturbances which may bring the topologically separate parts of the magnetic configuration closer. At the interface between the two flux tubes, a current sheet is generated, the magnetic field reconnects, and the magnetic energy is released in the process. This type of magnetic dissipation occurs not only when neighbouring magnetic field lines are oppositely directed but also when the field lines are inclined at a non zero angle.

Astrophysics and Space Science **250:** 147–162, 1997.

Resonant absorption of the Alfvén waves in an inhomogeneous plasma has been suggested as a means of driving current and plasma heating in the toroidal devices (Tataronis and Grossman, 1973; Chen and Hasegawa, 1974; Kapparaff and Tataronis, 1975; Mett and Taylor, 1992; Pandey *et al.*, 1995). In the context of coronal plasma heating such an investigation was started by Ionson (1978). Alfvén waves can play a dominant role in the heating of the coronal plasma since these waves are hardly attenuated in the transition region and thus can propagate very easily in the corona (e.g., Sakurai *et al.*, 1991a, 1991b; Hollweg, 1981; Goossens, 1991; Poedts and Kerner, 1992; Steinolfson and Davila, 1993; Goossens *et al.*, 1995). Grossman and Smith (1988) showed that these waves can be dissipated very effectively by means of resonant absorption in an inhomogeneous plasma. Later, the resonant absorption became the subject of immense study (e.g., Hollweg, 1990; Poedts *et al.*, 1990; Erdélyi and Goossens, 1994).

Although several studies exist on linear MHD waves, a few people have really put effort on its nonlinear counterparts. It is known that Alfvén waves can dissipate through the nonlinear interaction with the nonuniform ambient plasma. The nonlinear interaction of magnetohydrodynamic waves has been carried out by Kaburaki and Uchida (1971); Chiu and Wentzel (1972); Uchida and Kaburaki (1974); Barnes and Hollweg (1974) and Hollweg (1992). It has been found that Alfvén waves can decay into magnetosonic waves which then easily dissipates the energy in the corona. However, the full nonlinear problem does not yet seem to be within reach of analytical treatment. Therefore, we perform numerical simulation in the framework of nonlinear resistive MHD to study the effects of photospheric footpoint motion (Karpen *et al.*, 1991; Choudhuri *et al.*, 1993a,b). Recently Murawski *et al.* (1996) studied this problem but they considered only 1D magnetic field. Parhi *et al.* (1996) treated the problem when the magnetic field is 2D considering first the uniform and smooth density, magnetic field profile and driver and then proceeded to steep profiles and tried to understand the effect of sheared magnetic field (e.g., Choe and Lee, 1992; De Bruyne and Hood, 1993) on the evolution and properties of slow, fast and Alfvén waves. In both Parhi *et al.* (1996) and Murawski *et al.* (1996) the conclusions were derived when the plasma had evolved for a short time. We modified the code and were able to run the code for longer time. Also we considered smaller Lundquist number $aV_a/\eta = 10^5$ instead of 10^8 as in Parhi *et al.* (1996) or Murawski *et al.* (1996) to decipher the structures more clearly. The profiles for density, magnetic field and driver were chosen to be neither very smooth nor very steep which are considered by Parhi *et al.* (1996) and Murawski *et al.* (1996). Thus, some of the interpretations became transparent. Also, we performed the animation which added to our understanding of the wave evolution and coronal heating of the plasma.

2. Basic Equations

The coronal plasma obeys the following compressible, time-dependent, resistive equations:

$$\frac{\partial \rho}{\partial t} + \nabla \cdot (\rho \mathbf{V}) = 0, \tag{1}$$

$$\frac{\partial (\rho \mathbf{V})}{\partial t} + \nabla \cdot [(\rho \mathbf{V})\mathbf{V}] = -\nabla p + \frac{1}{\mu}(\nabla \times \mathbf{B}) \times \mathbf{B}, \tag{2}$$

$$\frac{\partial \mathbf{B}}{\partial t} = \nabla \times (\mathbf{V} \times \mathbf{B}) - \nabla \times (\eta \nabla \times \mathbf{B}), \tag{3}$$

$$\frac{\partial e}{\partial t} + \nabla \cdot (e\mathbf{V}) = -p\nabla \cdot \mathbf{V} + \frac{\eta}{\mu}(\nabla \times \mathbf{B})^2, \tag{4}$$

$$\nabla \cdot \mathbf{B} = 0. \tag{5}$$

Here ρ is the gas density, **V** is the velocity, μ is the magnetic permeability, p is the gas pressure, **B** is the magnetic field, $e = p/(\gamma - 1)$ is the internal energy per unit volume, η is the magnetic diffusivity and γ, the ratio of specific heats, is $5/3$.

We consider a simple coronal loop modelled by a slab geometry (Parhi *et al.*, 1996). The y direction is along the height of the loop, the z direction corresponds to the azimuthal direction and the inhomogeneity occurs in the x direction. Thus the photosphere is parallel to the $x - z$ plane. We assume that all the three velocity components at equilibrium are zero. Also, the derivative of all quantities with respect to z, i.e., $\partial/\partial z$, vanishes but V_z and B_z, the z components of perturbed flow and magnetic field, are nonzero. $B_x = 0$ and B_y is described in the next section. Consequently, both Alfvén and cusp singularities are present in such plasma which have been recently studied by Parhi and Lakhina (1994) and Parhi *et al.* (1996).

3. Simulation Model

The simulations were performed with a 2.5 dimensional resistive MHD code. The detailed description about the code is given elsewhere (Parhi *et al.*, 1996). The code is fourth order accurate in space and second order accurate in time. The time integration utilises predictor-corrector method. Double precision quantities are used throughout the calculations.

The computational box $(-5a, 5a) \times (-8a, 8a)$ consists of 100 cells in both horizontal x and vertical y directions. This roughly corresponds to 10^4 km horizontally and 1.6×10^4 km vertically. We consider rigid wall and free-slip boundary conditions at the top and bottom of the simulation regions ($y = \pm 8a$): $V_y = 0$ and $\partial f/\partial y = 0$ for $f = \rho, p, \mathbf{B}, V_x$, and V_z. This appears to be a reasonable constraint because the motions in the solar corona cannot much affect the high density photosphere. At the remaining (x) boundaries we applied open (zero gradient) conditions for all of the variables. Different boundary condition can also be considered, viz. the line-tying condition $\mathbf{V}(x, y = \pm 8a, t) = 0$. We present all our numerical results for the Lundquist number $aV_a/\eta = 10^5$ (Poedts *et al.*, 1990). The expression for the equilibrium gas pressure $p_0(x)$ is derived from the equilibrium condition $p_0 + B_0^2/2\mu =$ const, resulting in a plasma β of 0.04 far outside the slab. When $B_{0z} \neq 0$, the shear produced in the z direction drives all the three waves which are coupled. Thus there is large difference when twist is present or absent. Under the coronal conditions $(c_s \ll V_a)$ a plasma motion in the fast and slow waves is mostly transverse and longitudinal respectively. As a consequence we can associate V_x, V_y and

$$V3 = (B_{0y}V_z - B_{0z}V_y)/(B_{0y}^2 + B_{0z}^2)^{1/2} \tag{6}$$

as independent representatives for fast, slow and Alfvén waves, respectively (Erdélyi and Goossens, 1994). It is easy to see that when $B_{0z} = 0$, $V3 = V_z$.

The equilibrium density $\rho_0(x)$ and the magnetic field $B_{0y}(x)$ along the y direction are prescribed as follows:

$$\rho_0(x) = \begin{cases} \rho_i, & |x| \leq a, \\ \\ \rho_e + (\rho_i/\rho_e - 1)\rho_e/\cosh^6(|x| - a), & |x| > a, \end{cases}$$

$$B_{0y}(x) = \begin{cases} B_i, & |x| \leq a, \\ \\ B_e + (B_i/B_e - 1)B_e/\cosh^6(|x| - a), & |x| > a, \end{cases}$$

where the indices i and e denote the quantities in the inner and outer region of the slab, respectively. $\rho_0(x)$ is a smeared top-hat profile. Note that the smearing starts just at $x = \pm a$. We consider $\rho_i/\rho_e = 5$ and for zero twist the ratio of Alfvén speeds $V_{ae}/V_{ai} = 3$. Thus $(B_e/B_i)^2 = 9/5$.

The magnetic profile $B_{0z}(x)$ adopted here is as follows:

$$B_{0z}(x) = cxe^{-x^2}, \tag{7}$$

where one can choose the amplitude factor c. The plasma experiences twist due to this magnetic field.

We study the effect of photospheric footpoint motions. Thus, at the bottom of the simulation region we impose a body force F_z along z direction as follows:

$$F_z(x, y = -8a, t) = F_d(x)\sin(\omega_d t),$$

$$F_d(x) = \begin{cases} F_d, & |x| \leq a, \\ \\ F_d/\cosh^6(|x| - a), & |x| > a. \end{cases}$$

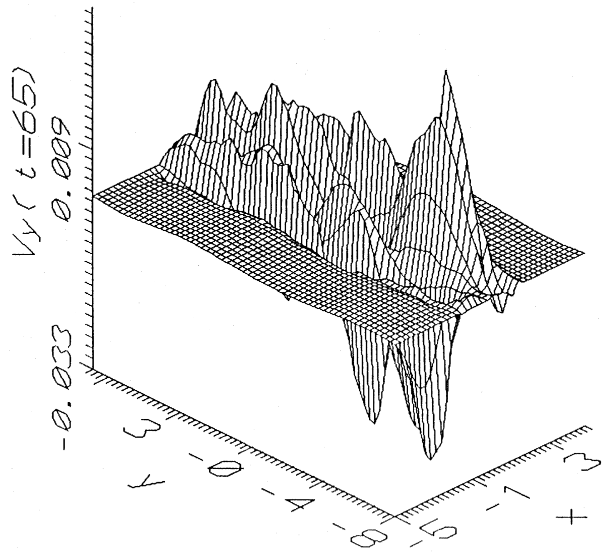

Figure 1. Spatial variation of V_y (corresponding to slow waves) at $t = 65\ a/V_{ae}$ for $c = 1.2\ V_{ae}\sqrt{\mu\rho_e}$ and $\omega_d = 0.2\ V_{ae}/a$. The driver has amplitude $F_d = 0.1\rho_e V_{ae}^2/a$.

Here, the constant F_d is the amplitude of the driver and ω_d is the driving frequency.

4. Results and Discussion

Here $\rho_0(x)$ and $B_0(x)$ are profiles which are neither very small nor very steep. As the external driver is turned on at $t = 0$, the oscillations are excited in the system. The driver is never turned off throughout the calculations. Resonant absorption is a process in an externally driven system. Steep gradient in V_y in Figure 1 is the signature of resonance layer where dissipation takes place. This is usually called cusp resonance (Parhi and Lakhina, 1994). There is no singularity or pseudo-singularity as described by Parhi *et al.* (1996) and Murawski *et al.* (1996). The width of this resonance layer is $\sim \eta^{1/3}$. As evolution progresses, the oscillations are expected to gradually become out of phase among neighbouring field lines as they oscillate with different eigenfrequency. This view is supported by watching the steep structure vanish if the simulation is continued for longer time. To convince ourselves clearly that the steep structures are not the singularity we run the simulation when the strength of the driver is very small (Figure 2). Consistent with our expectation we found that the amplitude of the steepness is very small.

Figure 3a describes the slow wave resonance at longer time. The frequency of the driver almost matches with that of the local Alfvén frequency in the corona. We know that in ideal MHD, the driven problem is governed by a set of differential equations that are singular at the point where the local Alfvén frequency matches

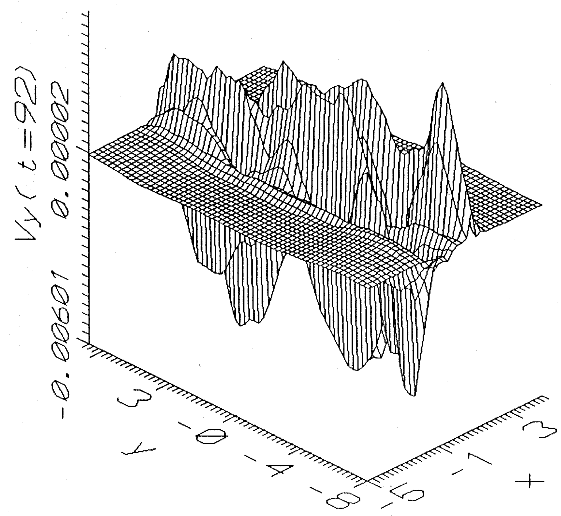

Figure 2. Spatial variation of V_y (corresponding to slow waves) at $t = 92\ a/V_{ae}$ for $c = 1.2$ and $F_d = 0.01\ \rho_e V_{ae}^2/a$. The driver has frequency $\omega_d = 0.2\ V_{ae}/a$.

the frequency of the wave in the corona. If there is no dissipation present in the system then the amplitude diverges at the resonance point exhibiting $1/x$ type singularity for the slow waves (Goedbloed, 1981). However, singularity is removed by the inclusion of finite viscosity/resistivity of the fluid. Dissipation takes place around the resonance point where the perturbation developes the large gradient. The width of the resonance layer is $\sim (\eta d\omega_A/dx)^{1/3}$ (Goossens *et al.*, 1995). In the present case we see the resonance along the slab at the edge of the simulation box. Since the steep profiles are symmetric with respect to $x = 0$ we see resonance at both the edges. The width of the resonance layer for the parameters of the present simulation can be calculated to be $\sim\ 0.1a$ when the governing parameters are considered which is in broad agreement with the width of the layer visible in the contour figure (Figure 3b). We see the evolution of slow waves in Figure 4 when there is no twist. The absence of twist leads to the slow decay of the oscillations due to phase mixing. However, in a twisted system the oscillations decay faster due to rapid phase mixing and we see only the remains of the oscillations which peak around the resonance point.

Now we discuss $V3$ which is a combination of V_y and V_z. In the absence of twist $V3$ reduces to V_z. We find Alfvén resonance at both edges of the slab (Figure 5). They are joined by a bridge like structure. Finite resistivity has completely removed the singularity. Note also that the thickness of the resonance layer in this case is more than that of the resonance layer developed in case of slow waves. This could be due to the larger frequency of Alfvén wave than that of the slow wave because the thickness of the layer depends on the frequency of the wave involved. The generation of the layer is not prominent close to the driver because the driver

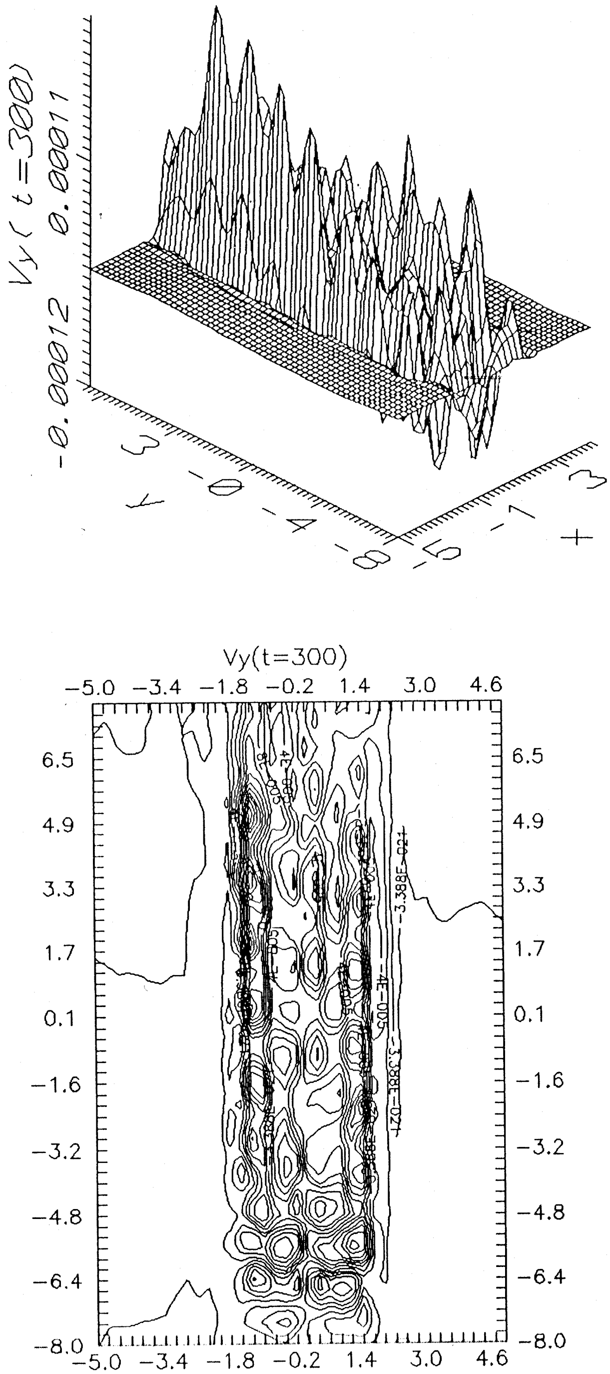

Figure 3. Spatial variation of V_y (corresponding to slow waves) at $t = 300\ a/V_{ae}$, for (a) $\omega_d = 0.9\ V_{ae}/a$, $F_d = 0.001\ \rho_e V_{ae}^2/a$, and $c = 0.6\ V_{ae}\sqrt{\mu\rho_e}$, (b) the contour plot of (a).

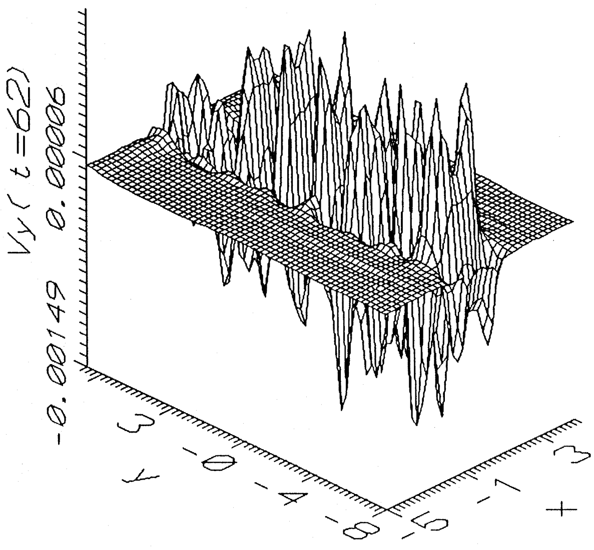

Figure 4. Spatial variation of V_y (corresponding to slow waves) at $t = 62\ a/V_{ae}$, for $\omega_d = 0.9\ V_{ae}/a$, $F_d = 0.001\ \rho_e V_{ae}^2/a$. There is no twist in this case.

interferes strongly with the evolution of the waves near the bottom boundary. Figure 6 describes the evolution of Alfvén wave when twist $c = 0.6V_{ae}\sqrt{\mu\rho_e}$. We see here the resonance layer at the center of slab apart from two layers at the edges. The driver excites the Alfvén wave which in turn excites the slow wave and both together modify the locations of the resonance layers. As the wave evolves in time (Figure 7) the resonance layer at the edges start to vanish. But the resonance layer in the middle of the slab undergoes slow deformation. As the excitation propagates in space transients decay and what we see as beautiful vortex like structures close to the bottom boundary is due to continuous pumping of energy due to driver.

Figure 8 describes the evolution of fast waves at $t = 150a/V_{ae}$. Comparison of Figure 8 with Figure 9 shows that larger twist arranges the pattern of fast modes more aligned along the tube. The distribution of fast waves is somewhat more uniform when the twist is less. More twist involves more pumping of energy. When the flux tube comes under increasingly more and more twist the magnetic pressure along x direction exceeds the magnetic tension along y direction. The tube no longer remains under tension and buckles. Thus we see the kink waves. Solar coronal loops are observed to be remarkably stable structures, but occasionally they lose stability and produce a flare. For many years this was a puzzle because normal MHD stability analysis shows that the flux tubes are unstable to kinking whenever they are twisted. Later it was observed that the line-tying of the ends of the loop in the dense photosphere is a dominant stabilizing effect. Thus any perturbation that is initiated in the corona vanish at the loop footpoints. The result is that the loop

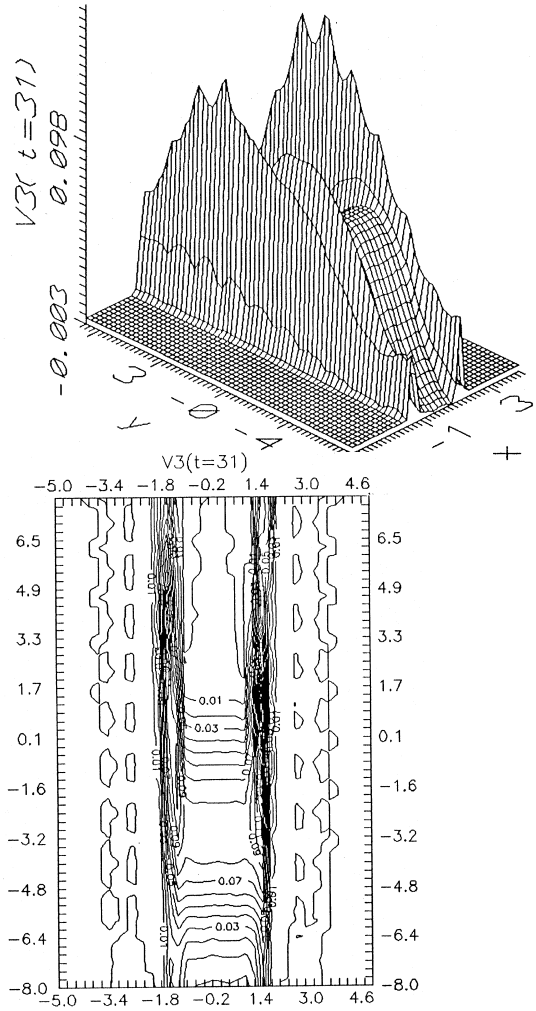

Figure 5. Spatial variation of $V3$ (corresponding to Alfvén waves) at $t = 31\ a/V_{ae}$ for (a) $c = 0$ and (b) the contour plot of (a). The driver has amplitude $F_d = 0.1\ \rho_e V_{ae}^2/a$ and frequency $\omega_d = 0.2\ V_{ae}/a$.

is stable when only slightly twisted but becomes kink unstable when the twist is large.

One can see from the x vs. J^2 plot at the equilibrium that there is a development of concentration of heating at the right edge of simulation box. Slowly as plasma evolves the two close humps denoting this concentration of heating gets separated and they appear on both edges of the flux tube as seen in Figures 10a and 10b. The twist makes the field lines incline at non-zero angle and facilitates the formation of current sheet. Obviously this has to be prominent in the region where the magnetic field has steep gradient. The current sheet which produces the heating gets distorted

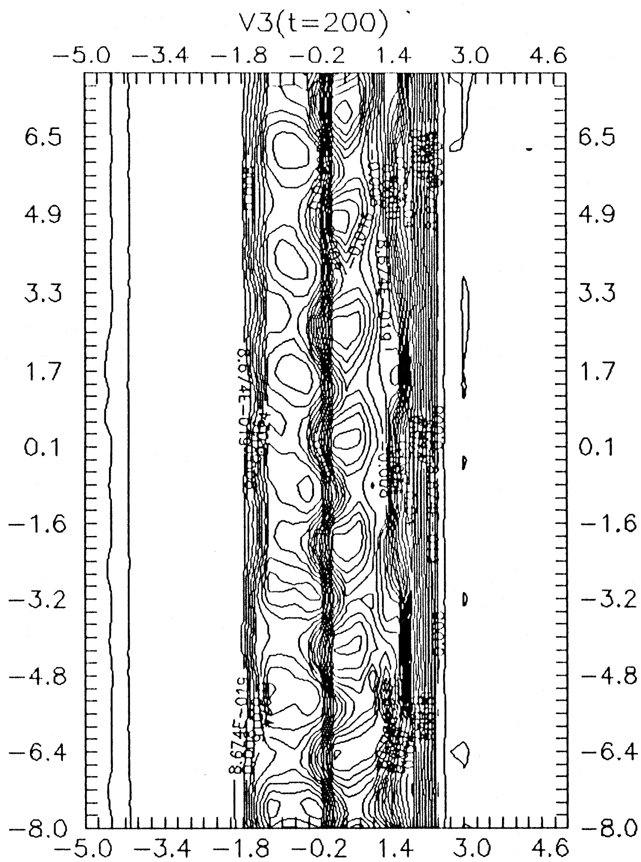

Figure 6. The contour picture of the spatial variation of $V3$ at $t = 200\ a/V_{ae}$ for the frequency of the driver $\omega_d = 0.9\ V_{ae}$ and its amplitude $F_d = 0.1\ \rho_e V_{ae}^2/a$ and twist $c = 0.6\ V_{ae}\sqrt{\mu\rho_e}$.

and fragments into two distinct current sheets at each edge. For larger value of twist these fragments seem to come closer towards the center of the flux tube (figure not shown). Thus it can be concluded that twist facilitates the distribution of heating in coronal tube.

5. Animation Observations

We first describe the observations derived from surface plots. We carried out the animation for $c = 0,\ 0.2\ V_{ae}\sqrt{\mu\rho_e}$, $\omega_d = 0.9\ V_{ae}/a$ and $F_d = 0.1\ \rho_e V_{ae}^2/a$ up to $t = 90\ a/V_{ae}$. For fast waves the perturbation travels faster outside the slab than inside the slab as a consequence of larger V_{ae} than V_{ai}. We observed patterns looking like standing waves formed at the top wall of the slab travelling backward. When there is no shear in the magnetic field initially created humps disappear and

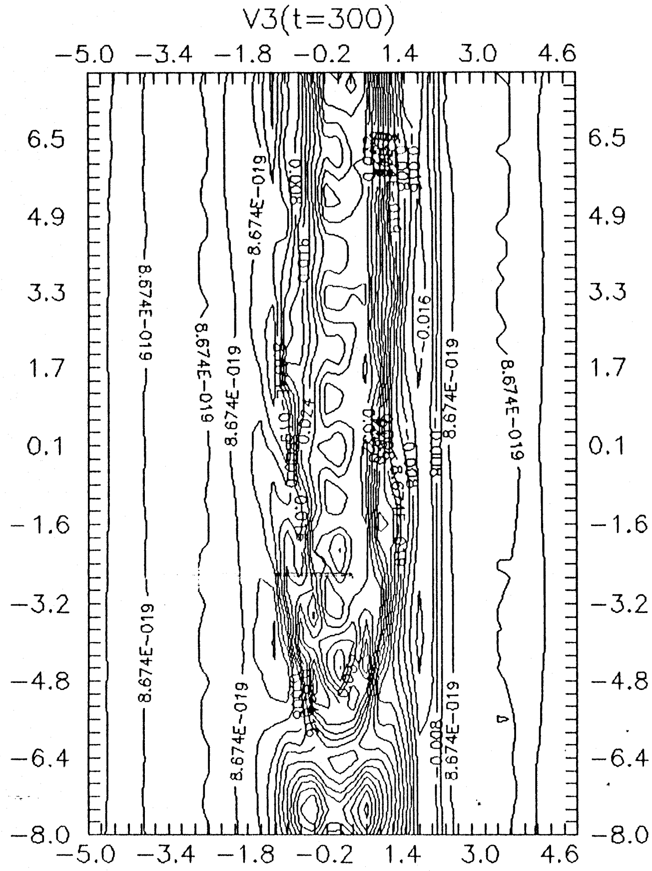

Figure 7. The contour picture of the spatial variation of $V3$ (corresponding to Alfvén waves) at $t = 300\ a/V_{ae}$ for twist $c = 0.1\ V_{ae}\sqrt{\mu\rho_e}$. The driver has amplitude $F_d = 0.1\ \rho_e V_{ae}^2/a$ and frequency $\omega_d = 0.9\ V_{ae}/a$.

new humps are formed as plasma evolves. But with little shear $(c = 0.2\ V_{ae}\sqrt{\mu\rho_e})$ no hump disappears, rather they oscillate. Roughly at $t = 60\ a/V_{ae}$, the waves appear to rebound from the top wall. The amplitude of the waves are at least a few times larger for $c = 0.2\ V_{ae}\sqrt{\mu\rho_e}$ than for $c = 0$.

The amplitude of Alfvén waves seems to retain same order of magnitude both for $c = 0$ and for $c = 0.2\ V_{ae}\sqrt{\mu\rho_e}$. Initially formed peaks at the right edge of the slab smooth out as plasma evolves because this is accompanied by a transition from short to large wavelength phenomenon and slowly it becomes difficult to recognise the peaks. Roughly at $t = 60\ a/V_{ae}$, smoothed humps dash against the top wall and degenerate into humps and valleys and travel backwards. Shear in the magnetic field makes this pattern more pronounced.

We now describe the observations derived from vector plots. Vortices formed initially at the bottom of the slab are slowly advected upwards and after some time

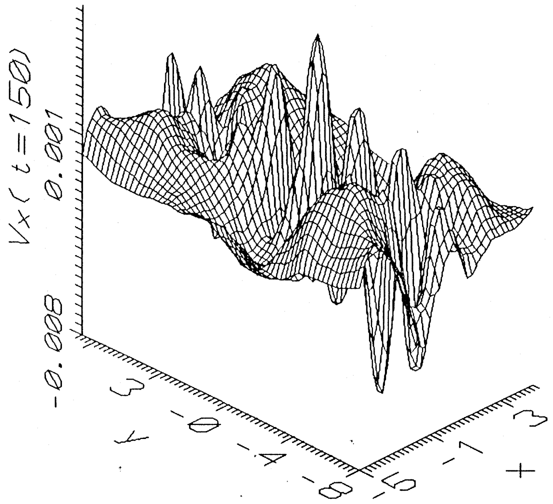

Figure 8. Spatial variation of V_x (corresponding to fast waves) at $t = 150\ a/V_{ae}$ for $F_d = 0.1\ \rho_e V_{ae}^2/a$. The driver has frequency $\omega_d = 0.9\ V_{ae}/a$ and twist $c = 0.6\ V_{ae}\sqrt{\mu\rho_e}$.

a few of them break down as they approach the top wall. The flow of plasma at the slab edges seems to be one way (positive, i.e., towards the observer) initially in the azimuthal direction but after a few Alfvén time plasma flows in both directions (positive and negative) because the system needs some time for effective interaction. Equally spaced vortices with clockwise or counter-clockwise rotations alternate among themselves in the slab. These vortices are nothing but $\mathbf{E} \times \mathbf{B}$ motions. It simply says current is generated locally and directional behaviour of the vortices at different sites even at the same edge probably prohibits the cancellation of different localized currents and hence leads to the formation of current sheet.

More work in this direction is in progress. The results will appear in a forthcoming paper.

6. Conclusion

We have performed the numerical simulation of wave propagation in the solar corona due to footpoint motion in the photosphere. The footpoint motion has been mimicked by an external driver. The problem is studied for various ranges of the driver amplitude and frequency. The results suggest that the driver excites Alfvén wave and magnetosonic waves. Consequently, these waves are resonantly absorbed in the corona leading to coronal heating. It is clearly evident from the plot J^2 vs. x that the twist facilitates the formation of current sheet which produces the heating. The boundary layer of thickness $\sim \eta^{1/3}$ where waves are absorbed is clearly seen. Also, increase in the shear of the magnetic field causes the resonance layer to shift

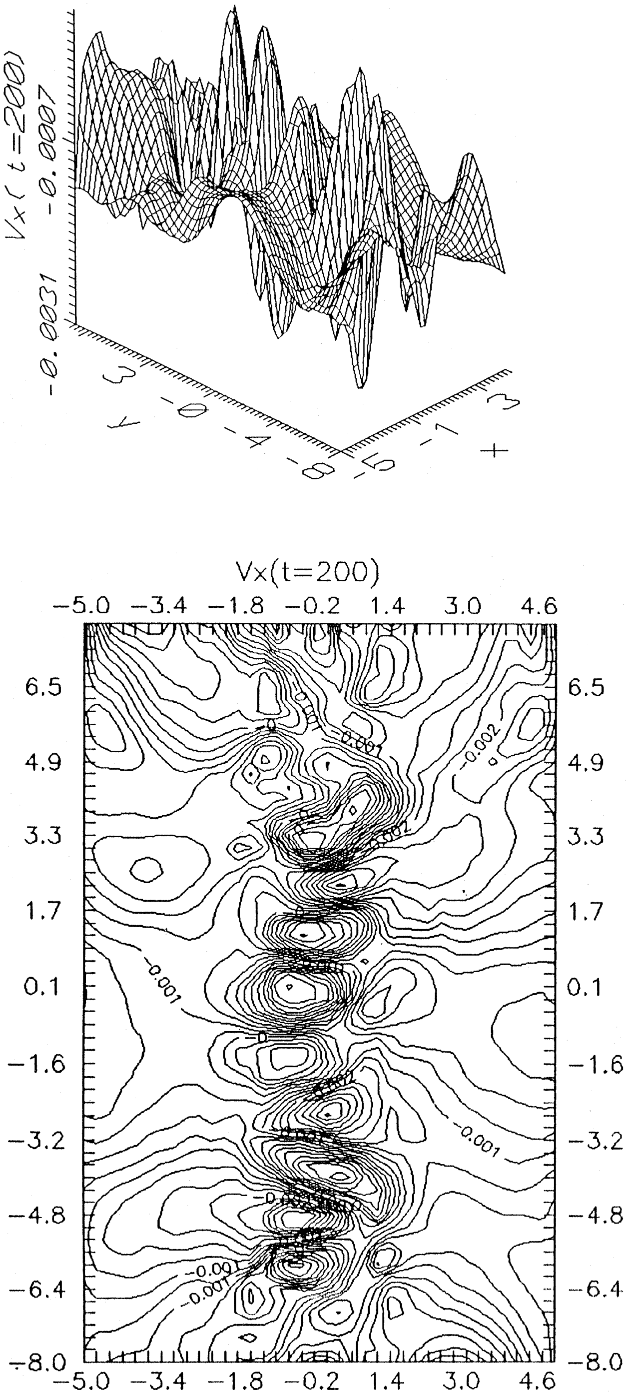

Figure 9. Spatial variation of V_x (corresponding to fast waves) at (a) $t = 200\ a/V_{ae}$ and (b) one contour plot of (a). The steep driver has frequency $\omega_d = 0.9\ V_{ae}/a$, amplitude $F_d = 0.1\ \rho_e V_{ae}^2/a$ and $c = 0.2\ V_{ae}\sqrt{\mu\rho_e}$.

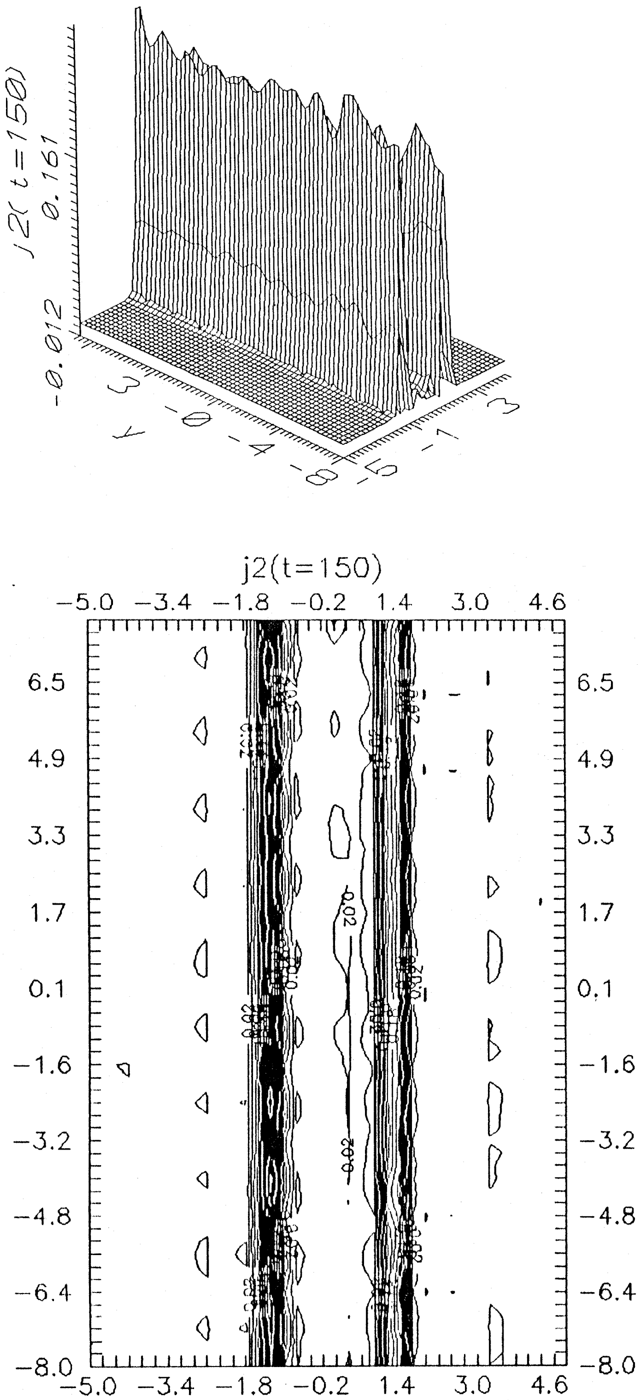

Figure 10. Spatial variation of heating J^2 at $t = 150\ a/V_{ae}$ for (a) $c = 0.2\ V_{ae}\sqrt{\mu\rho_e}$ and (b) one contour plot of (a). The driver has frequency $\omega_d = 0.9\ V_{ae}/a$ and amplitude $F_d = 0.1\ \rho_e V_{ae}^2/a$.

to the middle of the coronal tube. As the shear is increased beyond certain critical value, the resonance layer is seen to remain almost in the middle of the corona implying that the increase in the twist of the magnetic field determines the region where the resonance should occur.

Animation results indicate that magnetic twist (shear) plays very crucial role. Twisted fields sustain wave excitation for much longer time than the twist free case. It is expected as the twisted magnetic field has more energy than the untwisted fields. Therefore, the amplitude of the wave in the twisted case is larger compared to that in the twist free case. Next, study of the vector plot suggests the existence of current sheet. The motion of vortices indicates the orientation of **E** field. It suggests that the heating of the solar corona takes place via resonant absorption and the formation of current sheet.

Acknowledgements

PDB and MG acknowledge the support by the Onderzoeksfonds under the project OT/92/8 and by the "Federale Diensten voor Wetenschappelijke, Technische en Culturele Aangelegenheden" under grant IT/SC/07. SP, BP and GSL acknowledge the support of SERC school, DST, Govt. of India.

References

Barnes, A. and Hollweg, J.V.: 1974, *J. Geophys. Res.* **79**, 2302.
Cadez, V.M. and Ballester, J.L.: 1994, *Astron. Astrophys.*, in press.
Chen, L. and Hasegawa, A.: 1974, *Phys. Fluids* **17**, 1399.
Chiu, Y.T. and Wentzel, D.G.: 1972, *Astrophys. Space Sci.* **16**, 465.
Choe, G.S. and Lee, L.C.: 1992, *Sol. Phys.* **138**, 291.
Choudhuri, A.R., Auffret, H. and Priest, E.R.: 1993a, *Sol. Phys.* **143**, 49.
Choudhuri, A.R., Dikpati, M. and Banerjee, D.: 1993b, *Astrophys. J.* **413**, 811.
De Bruyne, P. and Hood, A.W.: 1993, *Sol. Phys.* **147**, 97.
Erdélyi, R. and Goossens, M.: 1994, *Astrophys. Space Sci.* **213**, 273.
Goedbloed, J.P.: 1983, *Lecture Notes on Ideal Magnetohydrodynamics*, Rijnhuizen Report 83-145, Nieuwegein, The Netherlands.
Goossens, M.: 1991, in: E.R. Priest and A.W. Hood (eds.), *Advances in Solar System Magnetohydrodynamics*, Cambridge Univ. Press, Cambridge, p. 137.
Goossens, M., Ruderman, M. and Hollweg, J.V.: 1995, *Sol. Phys.* **157**, 75.
Grossman, W. and Smith, R.A.: 1988, *Astrophys. J.* **332**, 476.
Hollweg, J.V.: 1981, *Sol. Phys.* **70**, 25.
Hollweg, J.V.: 1990, *Comp. Phys. Rep.* **12**, 205.
Hollweg, J.V.: 1992, *Astrophys. J.* **389**, 731.
Ionson, J.A.: 1978, *Astrophys. J.* **226**, 650.
Kaburaki, O. and Uchida, Y.: 1971, *Publ. Astron. Soc. Jpn.* **23**, 405.
Kapparaff, J.M. and Tataronis, J.A.: 1977, *J. Plasma Phys.* **18**, 209.
Karpen, J.T., Antiochos, S.K. and DeVore, C.R.: 1991, *Astrophys. J.* **382**, 327.
Mett, R.R. and Taylor, J.B.: 1992, *Phys. Fluids* **4**, 73.
Murawski, K., DeVore, C.R., Parhi, S. and Goossens, M.: 1996, *Planet Space Sci.* **44**, 253.
Pandey, B.P., Avinash, K., Sen, A. and Kaw, P.K.: 1995, *Phys. of Plasmas* **2**, 629.

Parhi, S. and Lakhina, G.S.: 1994, *Earth, Moon and Planets* **64**, 107.
Parhi, S., De Bruyne, P., Murawski, K., Goossens, M. and DeVore, C.R.: 1996, *Sol. Phys.*, **167**, 181.
Poedts, S., Goossens, M. and Kerner, W.: 1990, *Comp. Phys. Commun.* **59**, 95.
Poedts, S. and Kerner, W.: 1992, *J. Plasma Phys.* **47**, 139.
Rickard, G.J. and Priest, E.R.: 1994, *Sol. Phys.* **151**, 107.
Sakurai, T., Goossens, M. and Hollweg, J.V.: 1991a, *Sol. Phys.* **133**, 227.
Sakurai, T., Goossens, M. and Hollweg, J.V.: 1991b, *Sol. Phys.* **133**, 247.
Steinolfson, R.S.: 1991, *Astrophys. J.* **382**, 677.
Steinolfson, R.S. and Davilla, J.M.: 1993, *Astrophys. J.* **415**, 354.
Tataronis, J. and Grossman, W.: 1973, *Z. Phys.* **261**, 203.
Uchida, Y. and Kaburaki, O.: 1974, *Sol. Phys.* **35**, 451.
Wentzel, D.G.: 1974, *Sol. Phys.* **39**, 129.